Modified Second-Order Generalized Integrators With Modified Frequency Locked Loop for Fast Harmonics Estimation of Distorted Single-Phase Signals

Christoph M. Hackl, *Senior Member, IEEE*, and Markus Landerer

***Abstract*—This article proposes *modified second-order generalized integrators* (mSOGIs) for a fast estimation of all harmonic components of arbitrarily distorted single-phase signals, such as voltages or currents in power systems. The estimation is based on the internal model principle leading to an overall observer consisting of parallelized mSOGIs. The observer is tuned by pole placement. For a constant fundamental frequency, the observer is capable of estimating all harmonic components with prescribed settling time by choosing the observer poles appropriately. For time-varying fundamental frequencies, the harmonic estimation is combined with a *modified frequency locked loop* (mFLL) with gain normalization, sign-correct antiwindup, and rate limitation. The estimation performances of the proposed parallelized mSOGIs with and without mFLL are illustrated and validated by measurement results. The results are compared to standard approaches such as parallelized standard SOGIs (sSOGIs) and adaptive notch filters (ANFs).**

***Index Terms*—Amplitude estimation, frequency estimation, frequency-locked loop (FLL), phase estimation, second-order generalized integrator (SOGI).**

Notation

$\mathbb{N}, \mathbb{R}, \mathbb{C}, \mathbb{Q}$: natural, real, complex and rational numbers. For the following, let $n, m \in \mathbb{N}$. $\boldsymbol{x} := (x_1, \dots, x_n)^\top \in \mathbb{R}^n$: column vector (where $:=$ means "is defined as" and $^\top$ means "transposed"). $\mathbf{0}_n := (0, 0, \dots, 0)^\top \in \mathbb{R}^n$: zero vector. $\|\boldsymbol{x}\| := \sqrt{\boldsymbol{x}^\top \boldsymbol{x}}$: Euclidean norm of $\boldsymbol{x}$. $\boldsymbol{A} \in \mathbb{R}^{n \times m}$: real (non-square) matrix. $\mathrm{diag}(\boldsymbol{a}) \in \mathbb{R}^{n \times n}$: diagonal matrix with diagonal entries taken from vector $\boldsymbol{a} = (a_1, \dots, a_n)^\top \in \mathbb{R}^n$. $\mathrm{blockdiag}(\boldsymbol{A}_1, \dots, \boldsymbol{A}_n) \in \mathbb{R}^{nm \times nm}$: block diagonal matrix with matrix entries $\boldsymbol{A}_i \in \mathbb{R}^{m \times m}$, $i \in \{1, \dots, n\}$.

Manuscript received February 13, 2019; revised May 29, 2019; accepted July 28, 2019. Date of publication September 1, 2019; date of current version December 13, 2019. Recommended for publication by Associate Editor X. Wang. *(Christoph M. Hackl and Markus Landerer contributed equally to this work.) (Corresponding author: Christoph M. Hackl.)*

C. M. Hackl is with the Laboratory for Mechatronic and Renewable Energy Systems (LMRES) and with the Department of Electrical Engineering and Information Technology, Munich University of Applied Sciences (MUAS), 80335 Munich, Germany (e-mail: christoph.hackl@hm.edu).

M. Landerer is with the research group "Control of Renewable Energy Systems (CRES)", Munich School of Engineering, Technical University of Munich, 85748 Garching, Germany and with the Laboratory for Mechatronic and Renewable Energy Systems (LMRES), Munich University of Applied Sciences (MUAS), 80335 Munich, Germany. (e-mail: markus.landerer@tum.de).

Color versions of one or more of the figures in this article are available online at http://ieeexplore.ieee.org.

Digital Object Identifier 10.1109/TPEL.2019.2932790

I. Introduction

A. Motivation and Literature Review

In view of the increasing number of decentralized generation units with power electronics-based grid connection and the decreasing number of large-scale generators, the overall inertia in the grid is diminishing. This results in faster and more abrupt frequency fluctuations and significant harmonic distortion of physical quantities (such as currents or voltages) of the power system [1]. Fast frequency fluctuations endanger stability of the power grid. Significant harmonic distortions of voltages and currents can degrade power quality and lead to damage or even destruction of grid components. To be capable of taking appropriate countermeasures such as 1) improving system stability and power quality and 2) compensating for such deteriorated operation conditions, it is crucial to detect and estimate fundamental and higher harmonic components of the considered quantities in real time as fast and accurate as possible. Modern power electronic devices (e.g., flexible ac transmission systems or grid-connected converters of decentralized renewable energy systems) can then be used to implement such countermeasures. That is why, grid state estimation became of particular interest to the research community in the past years and has been studied extensively (see e.g., [2]–[24] to name a few).

It is well known that a signal with significant harmonic distortion can be decomposed and analyzed by the fast fourier transformation (FFT). However, this method requires a rather long computational time and a large amount of data to be processed [25, p. 320]. Usually, several multiples of the fundamental period ($\geq 200\mathrm{ms}$) are needed to estimate the harmonics with acceptable accuracy [7]; when the frequency must be estimated as well, the estimation time is even longer. For signals with negligible harmonic distortion, several well known and rather fast methods are available [26, Ch. 4], such as *second-order generalized Integrator (SOGI)* or *adaptive notch filters (ANF)* with and without *phase-locked loop (PLL)* [21] or *frequency locked-loop (FLL)* [2], [6]. For signals with significant harmonic distortion, these approaches fail and have to be extended by the parallelization of several SOGIs (see e.g., [6]–[8], [13], [24]) or several ANFs (see e.g., [3], [4]); each of those being capable of estimating the individual harmonics separately. However, the resulting estimation system is highly nonlinear (in particular in combination with FLL or PLL) and difficult to tune. The estimation speed is usually faster than those of FFT approaches

but still rather slow. Other estimation approaches use adaptive linear Kalman filters [27], SOGIs in combination with discrete Fourier transforms [28], adaptive Luenberger observers [29] (in transformed coordinates), or circular limit cycle oscillators [30].

A comparison of estimation speed and estimation accuracy mainly focuses on fundamental parameters and frequency. A comparison of all the results presented in the contributions above yields that the estimation speeds vary between 40–1200 ms. The estimation speed depends on the tuning of the estimation algorithms and the operation conditions (such as changing harmonics with varying amplitudes, phases, and frequencies) during the estimation process. In particular, when the frequency is changing abruptly, the overall estimation process is drastically decelerated. The FLL can be considered as the bottleneck of grid state estimation. Moreover, the performance of the estimation of the individual harmonics is mostly not discussed and evaluated.

Exceptions are the contributions [3], [6], and [7]; which explicitly discuss and show the estimation performance of the parallelized SOGIs and ANFs, respectively, for *each* considered harmonic component. For example, in [6], the proposed parallelized SOGIs with FLL (called MSOGI-FLL) are capable of extracting fundamental frequency and amplitudes and phases of a prespecified number n of harmonics $\nu \in \{\nu_1, \ldots, \nu_n\}$. Local stability analysis and tuning of the parallelized SOGIs and FLL were thoroughly discussed: The gain k_ν of the ν-th SOGI should be chosen as $k_\nu = \frac{1}{\nu}\sqrt{2} < \frac{1}{\nu}2$ which represents a "tradeoff between settle time, overshooting, and harmonic rejection" [6]. Simulation and measurement results were presented for three-phase signals. Six harmonics (including fundamental positive sequence) and the fundamental frequency were correctly estimated. The estimation speeds for the individual harmonics vary between 40–140 ms. Frequency estimation takes about 300 ms to settle at a constant value. In [7], a similar idea is proposed. The proposed algorithm is also based on parallelized SOGIs but a FLL has not been implemented. If the frequency is known, the method is capable of estimating the harmonics in approximately 40–60 ms.[1] Only simulation results were presented for seven harmonics. No results were presented when the frequency is unknown and varying. Implementation and tuning of the parallelized SOGIs are hardly discussed. In [3], parallelized ANFs with FLL are implemented. For a constant (estimated) frequency, a complete stability proof for the parallelized structure is presented showing that stability is preserved if all gains are chosen positive. The parallelized ANFs with FLL are implemented in MATLAB/Simulink to estimate a signal with six harmonic components (including fundamental). The fundamental frequency of the considered signal undergoes step-like changes of $+4$ and -2 Hz. Frequency and harmonics estimation errors tend to zero; but the estimation speed is rather slow and varies between 1–1.5 s.

The (parallelized) SOGIs and ANFs rely on a precise estimate of the fundamental (angular) frequency for proper functionality. If the frequency is known *a priori*, it can be fed directly to the parallelized systems. Otherwise, the observers must be combined with a FLL (or PLL), which allows to additionally estimate the fundamental angular frequency online. Since the FLL estimation depends on the harmonic amplitudes of the input signal, [6], [14], [16] propose a *gain normalization* (GN) which robustifies the frequency estimation. Nevertheless, due to its nonlinear and time-varying dynamics, the tuning of the overall estimator consisting of parallelized SOGIs or ANFs and FLL is a nontrivial task. As a rule of thumb (coming from a steady-state derivation of the FLL adaption law), the tuning of the FLL should be slow compared to the dynamics of the parallelized SOGIs or ANFs and, therefore, significantly degrades the settling time of the overall estimation system [9]. Apart from that, negative estimates of the angular frequency lead to instability. In this context, [11] describes a saturation of the estimated angular frequency to avoid a sign change. However, this saturation does not necessarily 1) ensure convergence of the estimation error or 2) accelerate the transient response of the FLL. In [23], the FLL is extended by output saturation and antiwindup (AWU) to avoid too large estimation values. But the proposed AWU strategy comes with an additional feedback gain (tuning parameter), which, if not properly chosen, endangers stability. Other approaches for frequency detection are based on PLL [10], [12], [18], [20], [21] which can be combined with SOGIs as well. PLL approaches are not considered in this article.

The remainder of this article focuses on modifications of the parallelized "standard SOGIs (sSOGI)" and the "standard FLL (sFLL)" as introduced in [2] and [6] which will allow to improve estimation speed and estimation accuracy. Key observation which motivates the modifications is that all papers above do only consider one single tuning factor (gain) for individual SOGI design. This single tuning factor limits the possible estimation performance. Therefore, this article proposes a *modified* (generalized) algorithm which achieves a prescribed settling time of the estimation process. It is capable of estimating amplitudes, angles, and angular frequencies of all harmonic components of interest in real time. The proposed algorithm consists of parallelized *modified* SOGIs tuned by pole placement. The modified SOGIs come with *additional* feedback gains (additional tuning parameters) which provide the required degrees of freedom to ensure a desired (prescribed) settling time. Since the sFLL was derived for the standard SOGI only (as shown in [6] or [8]), also a *modified* FLL is proposed to guarantee functionality in combination with the parallelized modified SOGIs. The article's novelty is characterized by the following contributions.

1) *Modification (generalization)* of standard SOGIs (sSOGIs) to *modified SOGIs (mSOGIs)* with *prescribed settling time* (see Sections II-A and II-B).
2) *Parallelization* of the mSOGIs and their *tuning by pole placement* (see Section II-C).
3) *Modification (generalization)* of the sFLL to the *modified FLL (mFLL)* with phase-correct adaption law, sign-correct AWU strategy, and rate limitation for enhanced functionality in combination with the proposed mSOGIs (see Section III).
4) *Implementation and validation* of the proposed estimation algorithm by simulation and measurement results and *comparison* of the estimation performances of parallelized mSOGIs, sSOGIs, and ANFs *with* and *without* FLL (see Section IV).

[1]Note that, the authors state that the estimation takes less than 20 ms, which seems not correct as can be observed in Figs. 6 and 8 in [7].

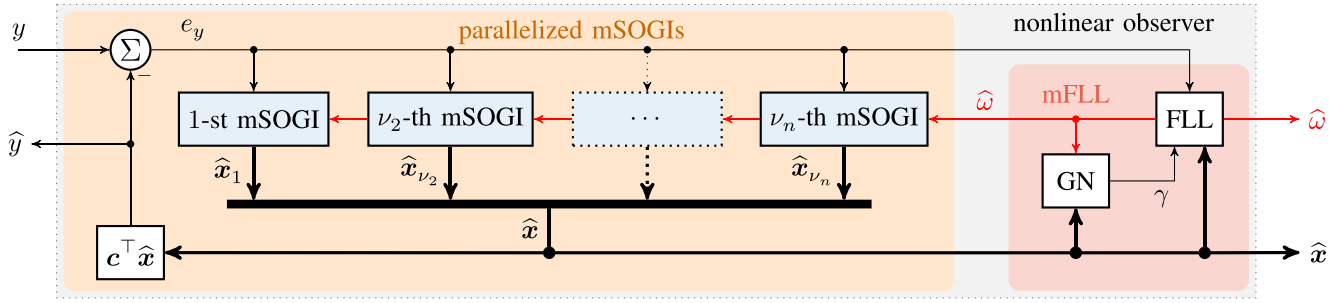

Fig. 1. Block diagram of the nonlinear observer consisting of parallelized mSOGIs and modified FLL (mFLL) with GN.

B. Problem Statement

Single-phase grid signals (e.g., voltages or currents) with significant and arbitrary harmonic distortion are to be estimated. The considered signals are assumed to have the following form:

$$\forall\, t \geq 0\colon \quad y(t) := \sum_{\nu \in \mathbb{H}_n} \underbrace{a_\nu(t) \cos\big(\phi_\nu(t)\big)}_{=:y_\nu(t)} \tag{1}$$

with $\mathbb{H}_n := \{1, \nu_2, \ldots, \nu_n\} \subset \mathbb{Q}_{>0}$, fundamental amplitude a_1, harmonic amplitudes $a_{\nu_2}, \ldots, a_{\nu_n} \geq 0$, and angles ϕ_ν (in rad), respectively; where $\nu \in \mathbb{H}_n$ indicates the ν-th harmonic component (per definition $\nu_1 := 1$). Observe that ν does not necessarily need to be a natural number or larger than one; any rational number is admissible as well (e.g. $\nu_2 = 5/3$ or $\nu_3 = 1/5$). To consider the general case[2], the phase angles

$$\forall \nu \in \mathbb{H}_n\ \forall t \geq 0: \qquad \phi_\nu(t) = \int_0^t \nu\, \omega\,(\tau)\, \mathrm{d}\tau + \phi_{\nu,0}$$

of the ν-th harmonic component depend on the time-varying angular *fundamental* frequency $\omega(\cdot) > 0\,\mathrm{rad\,s^{-1}}$ and the initial harmonic angle $\phi_{\nu,0} \in \mathbb{R}$.

The two main problems to be solved are 1) estimation of all amplitudes $\widehat{a}_\nu$ and angles $\widehat{\phi}_\nu$, such that after a *prescribed (specified) settling time* $t_{\mathrm{set}} > 0\,\mathrm{s}$, estimated signal

$$\widehat{y}(t) := \sum_{\nu \in \mathbb{H}_n} \underbrace{\widehat{a}_\nu(t) \cos\big(\widehat{\phi}_\nu(t)\big)}_{=:\widehat{y}_\nu(t)} \tag{2}$$

(indicated by " $\widehat{\ }$ ") and original signal y do not differ more than a given threshold $\varepsilon_y > 0$, i.e., $|y(t) - \widehat{y}(t)| \leq \varepsilon_y$ for all $t \geq t_{\mathrm{set}}$ and 2) asymptotic tracking (estimation) of the fundamental angular frequency ω by the estimate $\widehat{\omega}$, i.e., $\lim_{t\to\infty} \omega(t) - \widehat{\omega}(t) = 0$.

C. Principle Idea of Proposed Solution

The principle idea of the proposed solution is illustrated in Fig. 1. The depicted block diagram is fed by the input signal y to be estimated. All subsystems of the overall nonlinear observer are shown. The outputs of the block diagram are the respective estimated components of the input signal (see Section I-B). One can summarize: For $\nu \in \mathbb{H}_n$, the overall nonlinear observer consists of the following subsystems.

1) A *parallelization* of *modified second-order generalized integrators (mSOGIs)* to estimate amplitude and phase of each of the harmonic components of the input signal y. The ν-th mSOGI will output the estimated state vector

$$\widehat{\boldsymbol{x}}_\nu := \big(\widehat{x}_\nu^\alpha,\, \widehat{x}_\nu^\beta\big)^\top = \big(\widehat{y}_\nu,\, \widehat{q}_\nu\big)^\top$$

compromising estimates of in-phase and quadrature signals of the ν-th harmonic component, i.e., $\widehat{y}_\nu = \widehat{x}_\nu^\alpha$ and $\widehat{q}_\nu = \widehat{x}_\nu^\beta$, respectively. All n estimated signal vectors $\widehat{\boldsymbol{x}}_\nu$ are merged into the overall estimation vector

$$\widehat{\boldsymbol{x}} := \Big(\underbrace{(\widehat{y}_1, \widehat{q}_1)}_{=:\widehat{\boldsymbol{x}}_1^\top}, \underbrace{(\widehat{y}_{\nu_2}, \widehat{q}_{\nu_2})}_{=:\widehat{\boldsymbol{x}}_{\nu_2}^\top}, \ldots, \underbrace{(\widehat{y}_{\nu_n}, \widehat{q}_{\nu_n})}_{=:\widehat{\boldsymbol{x}}_{\nu_n}^\top}\Big)^\top \in \mathbb{R}^{2n}. \tag{3}$$

The output signal $\widehat{y} = \sum_{\nu\in\mathbb{H}_n} \widehat{y}_\nu = \boldsymbol{c}^\top \widehat{\boldsymbol{x}}$ represents the estimate of the input signal y and is established by the sum of all estimates of the in-phase signals $\widehat{y}_\nu = \widehat{x}_\nu^\alpha$ of the mSOGIs.

2) A *modified FLL (mFLL)* to obtain the estimate $\widehat{\omega}$ of the fundamental angular frequency ω. The mFLL depends on estimation input error $e_y := y - \widehat{y}$, estimation vector $\widehat{\boldsymbol{x}}$ and estimated angular frequency $\widehat{\omega}$, and is tuned by the gain Γ.

Sections II and III introduce the different subsystems (i.e., mSOGIs and mFLL) illustrated in Fig. 1 and explain in more detail their contribution to the proposed solution.

II. In-Phase and Quadrature Signal Estimation

The key tool to estimate in-phase and quadrature signals of a measured sinusoidal signal is a SOGI [26, App. A]. Their parallelization in combination with a FLL (see Section III) allows to detect all harmonic components and the fundamental frequency.

A. Modified SOGI (mSOGI) for ν-th Harmonic Estimation

To achieve estimation with *prescribed* performance, a *modified* SOGI (mSOGI) as shown in Fig. 2 must be introduced. Its dynamics are given by the following time-varying

[2]Note that in (1), time-varying amplitudes (of each harmonic component) *and* time-varying angles are considered. The typical assumption (see, e.g. [26, Appendix A]) of a *constant* fundamental angular frequency $\omega > 0$ such that $\phi_\nu(t) = \nu\omega t$ is *not* imposed, since it is not true in general.

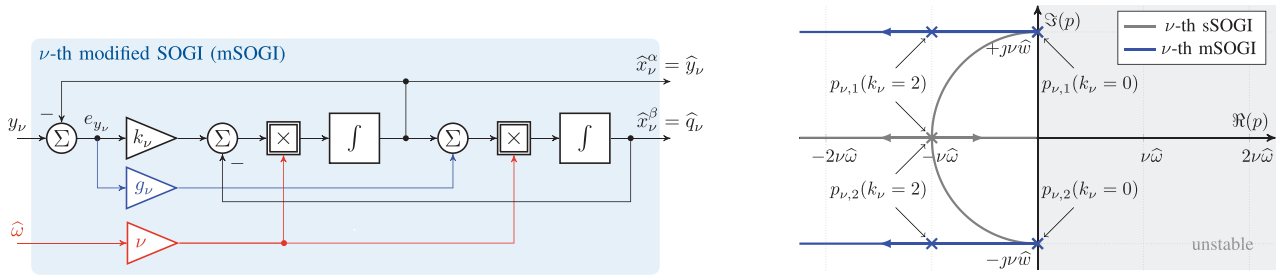

(a) Block diagram of ν-th mSOGI with *two* tuning parameters k_ν and g_ν. (block diagram of ν-th sSOGI is obtained by setting $g_\nu = 0$)

(b) Root loci of sSOGI (——, i.e. $g_\nu = 0$ in (4)) and mSOGI (——, i.e. $g_\nu = -\frac{k_\nu^2}{4}$ in (4)) for $k_\nu > 0$.

Fig. 2. mSOGI: (a) Block diagram and (b) root loci of ν-th sSOGI and ν-th mSOGI.

differential equation:

$$\left.\begin{aligned} \tfrac{\mathrm{d}}{\mathrm{d}t}\widehat{\boldsymbol{x}}_\nu &= \widehat{\omega}(t)\overbrace{\begin{bmatrix} -\nu k_\nu & -\nu \\ \nu(1-g_\nu) & 0 \end{bmatrix}}^{=:\boldsymbol{A}_\nu(k_\nu,g_\nu)}\widehat{\boldsymbol{x}}_\nu + \widehat{\omega}(t)\overbrace{\begin{pmatrix} \nu k_\nu \\ \nu g_\nu \end{pmatrix}}^{=:\boldsymbol{l}_\nu(k_\nu,g_\nu)} y_\nu(t) \\ \widehat{y}_\nu &= \boldsymbol{c}_\nu^\top \widehat{\boldsymbol{x}}_\nu \end{aligned}\right\} \tag{4}$$

with arbitrary initial value $\widehat{\boldsymbol{x}}_\nu(0) = \widehat{\boldsymbol{x}}_{\nu,0} \in \mathbb{R}^2$ (mostly set to zero) and estimate $\widehat{\omega}$ of ω. The mSOGI in (4) comes with *two* gains, i.e. k_ν *and* g_ν, which allow (theoretically[3]) for a "limitless" tuning of its dynamic response; in contrast to the *standard SOGI (sSOGI)* [6] with only *one* gain k_ν [i.e., $g_\nu = 0$ in (4)].

For a *constant* angular frequency $\widehat{\omega}$, the poles of ν-th mSOGI and ν-th sSOGI are, respectively, given by

$$\begin{aligned} p_{\nu,1/2} &= -\tfrac{\nu\widehat{\omega}k_\nu}{2}\left(1 \pm \sqrt{1 - 4\tfrac{(1-g_\nu)}{k_\nu^2}}\right) \\ &= \begin{cases} -\frac{\nu\widehat{\omega}k_\nu}{2} \pm j\nu\widehat{\omega}, & \text{mSOGI: } g_\nu = -\frac{k_\nu^2}{4} \\ -\frac{\nu\widehat{\omega}k_\nu}{2}\left(1 \pm \sqrt{1 - 4\frac{1}{k_\nu^2}}\right), & \text{sSOGI: } g_\nu = 0 \text{ [6].} \end{cases} \end{aligned} \tag{5}$$

The special choice of the additional gain $g_\nu = -\frac{k_\nu^2}{4}$ in (5) is exemplary but highlights the key advantage of the mSOGI over the sSOGI: For any $k_\nu > 0$, the real parts of the poles $p_{\nu,1/2}$ in (5) can be chosen arbitrarily. Moreover, in contrast to the sSOGI, the capability of the mSOGI to "oscillate" with angular frequency $\nu\widehat{\omega}$ is preserved (see imaginary parts of $p_{\nu,1/2}$). The root loci of ν-th mSOGI (——) and ν-th sSOGI (——) are depicted in Fig. 2(b). Both SOGIs are stable for any $k_\nu > 0$. However, only the transient response of the mSOGI becomes faster and faster, the larger k_ν is chosen (in particular for $k_\nu \geq 2$). Whereas, for the sSOGI, increasing k_ν yields one pole approaching the imaginary axis and, thus, to larger and larger settling times of the system. For the sSOGI, the smallest settling time is obtained for $k_\nu = 2$ which clearly limits its tuning and its transient estimation performance. Moreover, this choice leads to two real poles at $-\frac{\nu\widehat{\omega}k_\nu}{2}$ and, hence, the sSOGI is *not* capable of "oscillating" at $\nu\widehat{\omega}$ by itself. As compromise, common tunings are $k_\nu = \sqrt{2}/\nu$ [6] or $k_\nu = 1$ [3].

To overcome the tuning limitation not allowing for a prescribed settling time, the mSOGI with the additional (second) gain g_ν must be used. This additional gain does *not* impair functionality but gives the necessary degree of freedom to enhance the transient performance. Only for the mSOGI, *both* closed-loop poles $p_{\nu,1/2}$ can be chosen arbitrarily.

[3]Noise sensitivity, sensor errors and Shannon's Theorem will limit the feasible tuning and achievable estimation performance.

B. Estimation Performance Comparison of sSOGI and mSOGI

If $\widehat{\omega} = \omega$, both SOGIs are capable of estimating in-phase signal $\widehat{y}_\nu = \widehat{x}_\nu^\alpha$ and quadrature signal $\widehat{q}_\nu = \widehat{x}_\nu^\beta$ of the ν-th harmonic signal $y_\nu(t) := a_\nu(t)\cos(\phi_\nu(t))$. The estimated amplitude

$$\widehat{a}_\nu(t) := \|\widehat{\boldsymbol{x}}_\nu(t)\| = \sqrt{\widehat{y}_\nu(t)^2 + \widehat{q}_\nu(t)^2} \tag{6}$$

is given by the norm of the estimated in-phase signal and its quadrature signal. The estimated phase angle is given by

$$\widehat{\phi}_\nu(t) = \operatorname{arctan2}\big(\widehat{y}_\nu(t),\, \widehat{q}_\nu(t)\big). \tag{7}$$

Hence, the parameters $\widehat{a}_\nu$ and $\widehat{\phi}_\nu$ of the ν-th harmonic can be detected online.

In Fig. 3, for a fundamental signal $y = y_1$ (i.e., $\nu = \nu_1 = 1$), the transient responses of a single sSOGI (with $g_1 = 0$) and a single mSOGI (with $g_1 = -\frac{k_1^2}{4}$) for fundamental signal estimation are shown in gray and blue, respectively. Four tunings of the gain k_1 are implemented and illustrated by different line types: $k_1 = 0.5$ (dotted), $k_1 = 1$ (dashed), $k_1 = 2$ (dash-dotted) and $k_1 = 10$ (solid). The larger k_1 is chosen, the faster is the transient response of the mSOGI. Moreover, for $k_1 = 2$ (dash-dotted) or $k_1 = 10$ (solid), settling times of, e.g., $t_{\text{set}} = 0.01$ s and $t_{\text{set}} = 0.005$ s can be guaranteed, respectively. In contrast to that, for the sSOGI, a prescribed settling time *cannot* be ensured, since one pole approaches the imaginary axis for large choices of k_1 [recall Fig. 2(b)]. In particular, the estimation of the quadrature component is slow (see e_q in Fig. 3) which degrades the detection speed of positive, negative, and zero sequences in three-phase signals (not considered in this article).

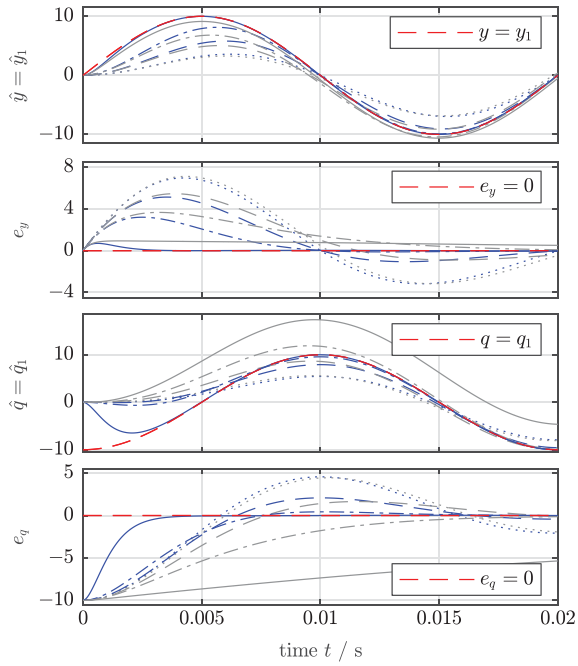

Fig. 3. Estimation performance comparison of sSOGI (·····, – – –, –·–·–, ——) and mSOGI (·····, – – –, –·–·–, ——) for four different tunings of gain $k_1 \in \{0.5, 1, 2, 10\}$, respectively. Signals shown are from top to bottom: input signal y_1 and its estimate $\widehat{y}_1$, estimation in-phase error $e_y = y_1 - \widehat{y}_1$, quadrature signal q_1 and its estimate $\widehat{q}_1$, and estimation quadrature error $e_q = q_1 - \widehat{q}_1$.

C. Parallelization of the mSOGIs

This far, the presented mSOGIs (or sSOGIs) can only estimate in-phase signal $\widehat{y}_\nu = \widehat{x}_\nu^\alpha$ and quadrature signal $\widehat{q}_\nu = \widehat{x}_\nu^\beta$ of the ν-th harmonic signal $y_\nu(t) := a_\nu(t)\cos(\phi_\nu(t))$. By parallelizing n of the mSOGIs (or sSOGIs; see Fig. 1), it is possible to extract in-phase and quadrature signal of each harmonic component y_ν for all $\nu \in \mathbb{H}_n$. For the parallelized sSOGIs, stability is preserved for a positive choice of all gains, i.e., $k_\nu > 0$ for all $\nu \in \mathbb{H}_n$ [3]. For the parallelized mSOGIs, proper pole placement will guarantee stability and allows to prespecify the settling time.

The idea of the parallelization can be motivated by recalling the *internal model principle* which states that "[e]very good regulator [or observer] must incorporate a model of the outside world being capable to reduplicate the dynamic structure of the exogenous signals which the regulator [or observer] is required to process" [31]. In the considered case, the exogenous signal y as in (1) can be reduplicated by the parallelization of n sinusoidal internal models [32, Ch. 20], with the dynamics

$$\left.\begin{aligned} \tfrac{\mathrm{d}}{\mathrm{d}t}\boldsymbol{x} &= \omega(t)\boldsymbol{J}\boldsymbol{x}, \qquad \boldsymbol{x}(0) = \boldsymbol{x}_0 \neq \boldsymbol{0}_{2n} \in \mathbb{R}^{2n} \\ y &= \underbrace{(1,\,0,\,1,\,0,\,\ldots,\,1,\,0)}_{=:\,\boldsymbol{c}^\top \in \mathbb{R}^{2n}}\boldsymbol{x} \end{aligned}\right\} \tag{8}$$

where $\boldsymbol{x} := \left(\boldsymbol{x}_1^\top, \ldots, \boldsymbol{x}_n^\top\right)^\top$, $\boldsymbol{x}_\nu := (x_\nu^\alpha,\, x_\nu^\beta)^\top$ for $\nu \in \mathbb{H}_n$

$$\boldsymbol{J} := \operatorname{blockdiag}\left(\overline{\boldsymbol{J}}, \nu_2\overline{\boldsymbol{J}}, \ldots, \nu_n\overline{\boldsymbol{J}}\right) \in \mathbb{R}^{2n\times 2n}$$

$$\text{and } \overline{\boldsymbol{J}} = \begin{bmatrix} 0 & -1 \\ 1 & 0 \end{bmatrix} = -\overline{\boldsymbol{J}}^\top = -\overline{\boldsymbol{J}}^{-1}. \tag{9}$$

The initial values $\boldsymbol{x}_0$ of the internal model in (8) allow to determine amplitude a_ν and angle ϕ_ν of the ν-th harmonic.

It can be shown[4] that, for constant $\omega > 0$ and differing harmonics $\nu_i \neq \nu_j$ for all $i \neq j \in \{1, \ldots n\}$, the overall internal model (8) is completely state observable. The observer consists of the parallelized mSOGIs (as introduced in (4) for the ν-th harmonic) and relies on the estimate $\widehat{\omega}$ of ω. The nonlinear observer dynamics are given by

$$\left.\begin{aligned} \tfrac{\mathrm{d}}{\mathrm{d}t}\widehat{\boldsymbol{x}}(t) &= \widehat{\omega}(t)\boldsymbol{J}\widehat{\boldsymbol{x}}(t) + \widehat{\omega}(t)\,\boldsymbol{l}\left(y(t) - \overbrace{\boldsymbol{c}^\top\widehat{\boldsymbol{x}}(t)}^{=\widehat{y}(t)}\right) \\ &= \widehat{\omega}(t)\left[\boldsymbol{J} - \boldsymbol{l}\boldsymbol{c}^\top\right]\widehat{\boldsymbol{x}}(t) + \widehat{\omega}(t)\,\boldsymbol{l}\,y(t) \\ \widehat{y}(t) &= \underbrace{\left(\boldsymbol{c}_1^\top, \boldsymbol{c}_{\nu_2}^\top, \ldots, \boldsymbol{c}_{\nu_n}^\top\right)}_{\overset{(4),(8)}{=}\boldsymbol{c}^\top}\widehat{\boldsymbol{x}}(t) \end{aligned}\right\} \tag{10}$$

with initial value $\widehat{\boldsymbol{x}}(t) = \widehat{\boldsymbol{x}}_0 \in \mathbb{R}^{2n}$. Observer state vector $\widehat{\boldsymbol{x}} \overset{(4)}{=} \left(\widehat{\boldsymbol{x}}_1^\top, \widehat{\boldsymbol{x}}_{\nu_2}^\top, \ldots, \widehat{\boldsymbol{x}}_{\nu_n}^\top\right)^\top \in \mathbb{R}^{2n}$ and observer gain vector

$$\boldsymbol{l} := \left(\boldsymbol{l}_1^\top, \boldsymbol{l}_{\nu_2}^\top, \ldots, \boldsymbol{l}_{\nu_n}^\top\right)^\top \overset{(4)}{=} (k_1,\, g_1,\, \ldots,\, \nu_n k_n,\, \nu_n g_n)^\top \in \mathbb{R}^{2n} \tag{11}$$

merge the individual state vectors $\widehat{\boldsymbol{x}}_\nu$ and gain vectors $\boldsymbol{l}_\nu$ of the ν-th mSOGI as in (4), respectively. The observer is tuned by pole placement. Hence, the gains in $\boldsymbol{l}$ can be determined by comparing the coefficients of the characteristic polynomial

$$\begin{aligned} \chi_{\boldsymbol{A}}(s) = &\prod_{i=1}^{n}\left(s^2 + \nu_i^2\right) - \sum_{i=1}^{n} g_i\nu_i^2 \prod_{\substack{k=1\\k\neq i}}^{n}\left(s^2 + \nu_k^2\right) \\ &+ s\sum_{i=1}^{n} k_i\nu_i \prod_{\substack{k=1\\k\neq i}}^{n}\left(s^2 + \nu_k^2\right) \end{aligned} \tag{12}$$

of the system matrix $\boldsymbol{A} := \boldsymbol{J} - \boldsymbol{l}\boldsymbol{c}^\top$ in (10) and the coefficients of a desired polynomial

$$\chi_{\boldsymbol{A}}^*(s) := \prod_{i=1}^{2n}(s - p_i^*) \tag{13}$$

with $2n$ prescribed stable roots (poles) p_i^* in the negative complex half-plane, i.e., $p_i^* \in \mathbb{C}_{<0}$, $i \in \{1, \ldots, 2n\}$. The resulting observer gain vector $\boldsymbol{l}$ is obtained as follows:

$$\boldsymbol{l} = \boldsymbol{S}\,\widetilde{\boldsymbol{p}}_{\boldsymbol{A}}^* \tag{14}$$

where $\boldsymbol{S} := \begin{bmatrix} \boldsymbol{S}_{1,1} & \cdots & \boldsymbol{S}_{n,1} \\ \vdots & \ddots & \vdots \\ \boldsymbol{S}_{1,n} & \cdots & \boldsymbol{S}_{n,n} \end{bmatrix}$ with $\boldsymbol{R}_j := \begin{bmatrix} 1 & 0 \\ 0 & -\frac{1}{\nu_j} \end{bmatrix}$ and

$$\boldsymbol{S}_{i,j} := (-1)^{i+1}\nu_j^{2(n-i)}\boldsymbol{R}_j \prod_{\substack{l=1\\l\neq j}}^{n}(\nu_j^2 - \nu_l^2)^{-1}$$

$$\text{and } \widetilde{\boldsymbol{p}}_{\boldsymbol{A}}^* := \left(-\sum_{i=1}^{2n} p_i^*,\ \sum_{i=1}^{2n} p_i^* \sum_{j=i+1}^{2n} p_j^* - \sum_{i=1}^{n}\nu_i^2 \right.$$
$$\left. -\sum_{i=1}^{2n} p_i^* \sum_{j=i+1}^{2n} p_j^* \sum_{k=j+1}^{2n} p_k^*,\ \ldots,\ \prod_{i=1}^{2n} p_i^* - \prod_{i=1}^{n}\nu_i^2\right)^\top. \tag{15}$$

[4] All proofs are available with the authors but omitted due to space limitations.

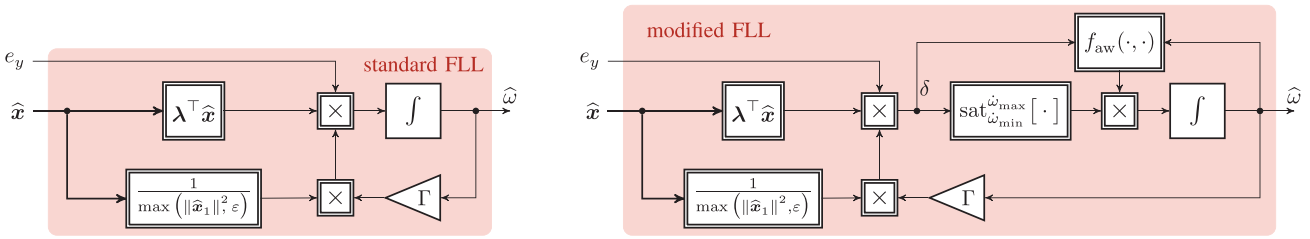

(a) sFLL with gain normalization and $\boldsymbol{\lambda} = (0, k_1, 0, \ldots, 0)^\top$.

(b) mFLL with gain normalization, sign-correct anti-windup strategy, rate limitation and $\boldsymbol{\lambda} = (-g_1, k_1, 0, \ldots, 0)^\top$.

Fig. 4. Angular frequency estimation with (a) sFLL and (b) mFLL.

It can be shown[4] that, for any positive (but possibly time-varying) angular frequency estimate, i.e., $\widehat{\omega}(t) \geq \varepsilon_\omega > 0$ for all $t \geq 0$, the closed-loop observer system (10) is bounded-input bounded-output stable *and* input-to-state stable Moreover, it can be shown[4] that, if $\widehat{\omega} \to \omega$, then the estimation state error $\boldsymbol{e}_x := \boldsymbol{x} - \widehat{\boldsymbol{x}} \to \mathbf{0}_{2n}$ decays *exponentially* to zero.

III. Frequency Estimation

For frequency estimation, usually a FLL is utilized. It can be considered as the bottleneck of grid state estimation [33].

A. Standard FLL (sFLL) and Modified FLL (mFLL)

The block diagram of the *sFLL* with gain normalization [3], [6], [16] is depicted in Fig. 4(a). The parallelized mSOGIs require a modification of the sFLL; otherwise frequency estimation will not work properly anymore. The block diagram of the proposed *mFLL* is shown in Fig. 4(b). In contrast to the sFLL, the mFLL is equipped with the modified (generalized) adaption law

$$\frac{\mathrm{d}}{\mathrm{d}t}\widehat{\omega} = f_{\mathrm{mFLL}}(\widehat{\omega}, \widehat{\boldsymbol{x}}, e_y) := f_{\mathrm{aw}}(\widehat{\omega}, \delta)\ \mathrm{sat}_{\dot{\omega}_{\min}}^{\dot{\omega}_{\max}}\left[\overbrace{\frac{\Gamma\,\widehat{\omega}\,e_y\,\boldsymbol{\lambda}^\top\widehat{\boldsymbol{x}}}{\max\left(\|\widehat{\boldsymbol{x}}_1\|^2, \varepsilon\right)}}^{=:\delta}\right] \tag{16}$$

with initial value $\widehat{\omega}(0) = \widehat{\omega}_0 > 0$. A proper choice of the initial value, e.g. $\widehat{\omega}_0 \in \{2\pi\,50, 2\pi\,60\}$, will be beneficial for functionality and adaption speed.

The mFLL in (16) depends on 1) the modified "selection" vector $\boldsymbol{\lambda} = (-g_1, k_1, 0, \ldots, 0)^\top$ to select both fundamental components $\widehat{\boldsymbol{x}}_1 = (\widehat{y}_1, \widehat{q}_1)^\top$ from $\widehat{\boldsymbol{x}}$ (in contrast to $\boldsymbol{\lambda} = (0, k_1, 0, \ldots, 0)^\top$ as used for the sFLL [6]), 2) the estimation state vector $\widehat{\boldsymbol{x}}$, 3) estimation error $e_y := y - \widehat{y}$ (difference between input y and estimated input $\widehat{y}$), 4) a sign-correct AWU decision function

$$f_{\mathrm{aw}}(\widehat{\omega}, \delta) := \begin{cases} 0, & \text{for } \left(\widehat{\omega} \geq \omega_{\max} \wedge \delta \propto \frac{\mathrm{d}}{\mathrm{d}t}\widehat{\omega} \geq 0\right) \\ & \vee \left(\widehat{\omega} \leq \omega_{\min} \wedge \delta \propto \frac{\mathrm{d}}{\mathrm{d}t}\widehat{\omega} \leq 0\right) \\ 1, & \text{else} \end{cases} \tag{17}$$

and (v) a rate limitation

$$\mathrm{sat}_{\dot{\omega}_{\min}}^{\dot{\omega}_{\max}}[\delta] := \begin{cases} \dot{\omega}_{\max}, & \delta > \dot{\omega}_{\max} \\ \delta, & \dot{\omega}_{\min} \leq \delta \leq \dot{\omega}_{\max} \\ \dot{\omega}_{\min}, & \delta < \dot{\omega}_{\min}. \end{cases} \tag{18}$$

Note that, in particular for severe voltage dips or low-voltage ride through (LVRT), the gain normalization by the denominator $\max(\|\widehat{\boldsymbol{x}}_1\|, \varepsilon)$ in (16) is essential and avoids a division by zero by introducing a minimal denominator value $\varepsilon > 0$. The modifications compared to the sFLL [i.e., (i), (iv), and (v)] enhance performance and stability of the overall observer (see Section III-B).

Finally, it should be noted that for the mFLL, it is beneficial to bandpass filter the signal δ in (16) to damp higher order harmonics and extract the fundamental component only (proportional to $e_{y_1}(-g_1\widehat{y}_1 + k_1\widehat{q}_1)$). A suitable bandpass filter is given by

$$F_{\mathrm{bpf}}(s) := \frac{\omega_{\mathrm{bpf}}}{s + \omega_{\mathrm{bpf}}} \cdot \frac{s}{s + \omega_{\mathrm{bpf}}}$$

which does not induce *any* phase lag at ω_{bpf}. A proper choice of the filter angular frequency is $\omega_{\mathrm{bpf}} = 2\pi f_{\mathrm{g}}$ with the nominal grid frequency $f_{\mathrm{g}} = 50\,\mathrm{Hz}$ or $f_{\mathrm{g}} = 60\,\mathrm{Hz}$.

B. Effects of the Modifications on Frequency Estimation

The sign-correct AWU strategy[5] in (17) guarantees that the estimated angular frequency $\widehat{\omega}$ remains bounded and positive for all time [see Fig. 5(a)]. Usually, the grid frequency ω does not exceed a certain interval; which can be exploited for frequency estimation as well: Frequency adaption shall be stopped (i.e. $\frac{\mathrm{d}}{\mathrm{d}t}\widehat{\omega} = 0$), when (i) the estimated angular frequency $\widehat{\omega}$ leaves the admissible interval, i.e. $\widehat{\omega} \notin (\omega_{\min}, \omega_{\max})$ with lower and upper limit $0 < \omega_{\min} < \omega_{\max}$, respectively [see Fig. 5(a)]; and (ii) the right-hand side of the adaption (16) has wrong sign (otherwise the estimation gets stuck at one of the limits).

The rate limitation (RL) in (18) prevents too fast adaption speeds [see Fig. 5(b)] and leads to a smoother adaption. Usually, $\dot{\omega}_{\min} = -\dot{\omega}_{\max}$ is a meaningful choice with $\dot{\omega}_{\max} = 2\pi\,10\,\mathrm{Hz}/1\,\mathrm{ms} \ldots 2\pi\,100\,\mathrm{Hz}/1\,\mathrm{ms}$. Concluding, the adaption law (16) guarantees that (i) the derivative of the estimated angular frequency is bounded, i.e., $\frac{\mathrm{d}}{\mathrm{d}t}\widehat{\omega}(t) \in \left[\dot{\omega}_{\min}, \dot{\omega}_{\max}\right]$, (ii) the estimated angular frequency is always positive (negative frequencies will endanger stability of the observer) and (iii) it is always bounded from below and above, i.e. $\widehat{\omega}(t) \in \left[\min(\widehat{\omega}_0, \omega_{\min}), \max(\widehat{\omega}_0, \omega_{\max})\right]$ for all $t \geq 0$. In Fig. 5(c), exemplary frequency adaption results are shown for four implementations of the adaption law (16): (a) without AWU and

[5]The proposed sign-correct antiwindup strategy does not require tuning of an additional feedback gain as e.g. in [23]. It is based on the simple idea of *conditional integration* [32, Section 10.4.1] and instability can *not* occur.

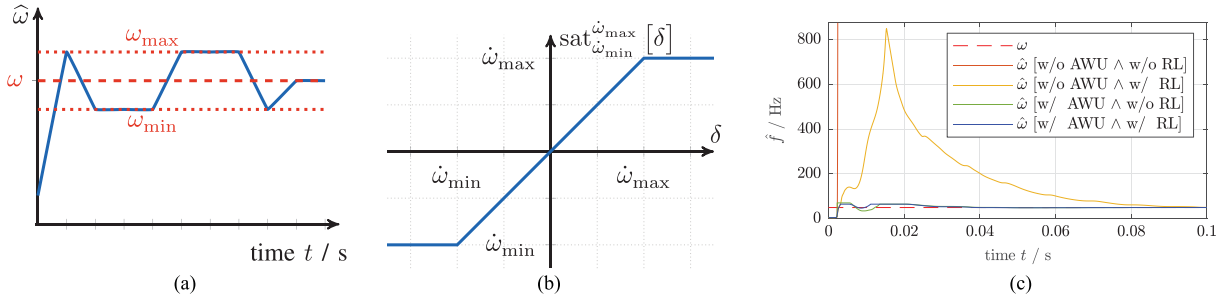

Fig. 5. Illustration of the modifications for the mFLL and their effects on frequency estimation. (a) Illustration of sign-correct AWU. (b) Illustration of the rate limitation. (c) Simulative comparison of modification effects.

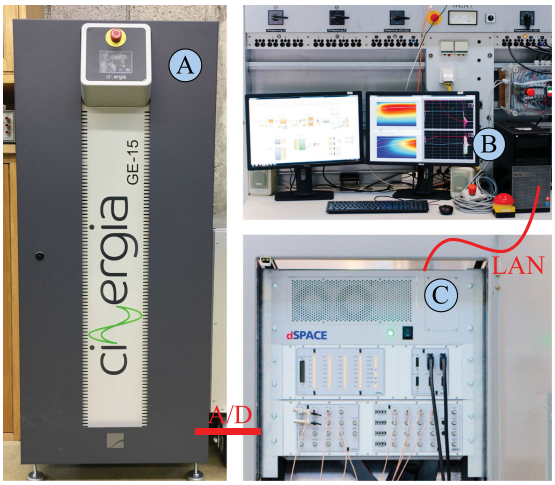

Fig. 6. Laboratory setup. (a) Cinergia grid emulator. (b) Host-PC. (c) dSPACE real-time system.

RL (*unstable*), (b) without AWU and with RL (*huge overshoot*), (c) with AWU and without RL (*less smooth*) and (d) with AWU and RL, respectively.

IV. Implementation and Measurement Results

To validate the proposed algorithms, measurements at a laboratory setup are carried out. The laboratory setup is shown in Fig. 6. For measurements, the voltage is produced by a grid emulator. These voltages are measured by a LEM DVL 500 voltage sensor and analog-to-digitally converted by the dSPACE A/D card DS2004. The measured signals are *not* filtered to avoid any phase lag due to filtering. The implementation is done via MATLAB/Simulink R2017a on the Host-PC. The executable observers are downloaded via LAN to the dSPACE Processor Board DS1007 and run in real time. The measurement data is captured and analyzed on the Host-PC after the experiment.

The implementation data of the conducted measurements is listed in Table I. Three estimation methods are implemented:

1) ——*single* mSOGI or *parallelized* mSOGIs *with* and *without* mFLL, i.e., observer (10) with $\boldsymbol{l}$ as in (14);
2) ——*single* sSOGI or *parallelized* sSOGIs *with* and *without* sFLL [6], i.e., observer (10) with $\boldsymbol{l} = \sqrt{2}\boldsymbol{c}$ (and $g_\nu = 0$ for all $\nu \in \mathbb{H}_n$);
3) ——*single* adaptive notch filter (ANF) or *parallelized* ANFs *with* and *without* FLL (as in [3][6]), i.e. observer (10) with $\boldsymbol{l} = \boldsymbol{c}$.

Their estimation performances are compared for the following *four* measurement scenarios:

1) Estimation of a *fundamental* input signal y with known and constant angular frequency (i.e., $\widehat{\omega}(t) = \omega(t) = 2\pi 50$ rad s^{-1} for all $t \geq 0$) but with (a) an amplitude jump (-75%) at $t_1 = 0.04$ s, (b) a phase jump ($+\pi/2$) at $t_2 = 0.08$ s, and (c) an amplitude jump ($+300\%$) *and* a phase jump ($-\pi/2$) at $t_3 = 0.12$ s. The measurement results for this scenario are shown in Fig. 7.
2) Estimation of a *fundamental* input signal y with unknown and time-varying fundamental angular frequency $\omega(\cdot)$ [i.e., $\widehat{\omega}_0 \neq \omega(0)$]. At $t_1 = 0.2$ s, the frequency jumps from 50 to 60 Hz. At $t_2 = 0.4$ s, the frequency jumps from 60 to 40 Hz *and* the signal undergoes an amplitude jump (-75%). The measurement results for Scenario (S_2) are shown in Fig. 8.
3) Estimation of an input signal y with *ten* harmonics. The angular frequency is known and constant (i.e., $\widehat{\omega}(t) = \omega(t) = 2\pi 50$rad s^{-1} for all $t \geq 0$) but the signal undergoes (a) an amplitude jump (-75%) at $t_1 = 0.04$ s, (b) a phase jump ($+\pi/2$) at $t_2 = 0.08$ s and (c) an amplitude jump ($+300\%$) *and* a phase jump ($-\pi/2$) at $t_3 = 0.12$ s. The results for this scenario are shown in Figs. 9 and 10.
4) Estimation of an input signal y with *ten* harmonics and unknown *and* time-varying fundamental angular frequency $\omega(\cdot)$ (i.e. $\omega h_0 \neq \omega(0)$). Similar to Scenario ($S_2$), at $t_1 = 0.2$ s, the frequency jumps from 50 to 60 Hz. At $t_2 = 0.4$ s, the frequency jumps from 60 to 40 Hz *and* the signal undergoes an amplitude jump (-75%). Figs. 11 and 12 depict the results for Scenario (S_4).

For Scenarios (S_1) and (S_3), the grid frequency ω is constant and known. Hence, frequency estimation (FLL) is disabled, i.e., the FLL integrator is multiplied by zero, and initialized with the value $\widehat{\omega}(0) = \omega$ of the real frequency. For Scenarios (S_1) and (S_2), only fundamental input signals are considered

[6]In [3], the FLL is implemented without GN and its gain γ is set to 80. The maximal signal amplitude, in the experiments used in [3], is $a_1 = 1$. Because the grid emulator cannot produce such low voltages and the FLL is driven without a GN, the FLL gain of the ANFs for scenarios (S_2) and (S_4) was adjusted in view of the larger amplitudes.

TABLE I
IMPLEMENTATION AND TUNING DATA FOR SCENARIOS (S_1)–(S_4)

Implementation	
sampling time	$h = 0.1\,\mathrm{ms}$
parallelized mSOGIs	
observer gains	$\boldsymbol{l}$ as in (14) [$\Longrightarrow\ \forall \nu \in \mathbb{H}_\nu$: $p^*_{1,2,\nu} = -\frac{3}{2} \pm \jmath\nu$]
mFLL	$\Gamma = 60$, $\varepsilon = 0.1$
anti-windup	$\omega_{\min} = 39\,\frac{\mathrm{rad}}{\mathrm{s}}$, $\omega_{\max} = 61\,\frac{\mathrm{rad}}{\mathrm{s}}$
rate limitation	$\dot{\omega}_{\max} = 2\pi \cdot 10 \cdot 10^3\,\frac{\mathrm{rad}}{\mathrm{s}^2}$, $\dot{\omega}_{\min} = -\dot{\omega}_{\max}$
parallelized sSOGIs [6]	
observer gains	$\boldsymbol{l} = \sqrt{2}\boldsymbol{c}$
sFLL	$\Gamma = 46$, $\varepsilon = 0.1$
parallelized ANFs [3]	
filter gains	$\boldsymbol{l} = \boldsymbol{c}$
FLL (as in [3])	$\gamma = 1$ (w/o gain normalizat.)
Scenario (S_1) with constant fundamental frequency	
observer order	2 ($n = 1$; fundamental)
obs. initial values	$\widehat{\boldsymbol{x}}_0 = \boldsymbol{0}_2$
FLL initial values	$\widehat{\omega}_0 = 2\pi\,50\,\frac{\mathrm{rad}}{\mathrm{s}} = \widehat{\omega}(t)$
Scenario (S_2) with varying fundamental frequency	
observer order	2 ($n = 1$; fundamental)
obs. initial values	$\widehat{\boldsymbol{x}}_0 = \boldsymbol{0}_2$
FLL initial values	$\widehat{\omega}_0 = 2\pi\,25\,\frac{\mathrm{rad}}{\mathrm{s}} \neq 2\pi\,50\,\frac{\mathrm{rad}}{\mathrm{s}}$
Scenario (S_3) with constant fundamental frequency	
observer order	20 ($n = 10$, i.e. 10 harmonics)
obs. initial values	$\widehat{\boldsymbol{x}}_0 = \boldsymbol{0}_{20}$
FLL initial values	$\widehat{\omega}_0 = 2\pi\,50\,\frac{\mathrm{rad}}{\mathrm{s}} = \widehat{\omega}(t)$
Scenario (S_4) with varying fundamental frequency	
observer order	20 ($n = 10$, i.e. 10 harmonics)
obs. initial values	$\widehat{\boldsymbol{x}}_0 = \boldsymbol{0}_{20}$
FLL initial values	$\widehat{\omega}_0 = 2\pi\,25\,\frac{\mathrm{rad}}{\mathrm{s}} \neq 2\pi\,50\,\frac{\mathrm{rad}}{\mathrm{s}}$

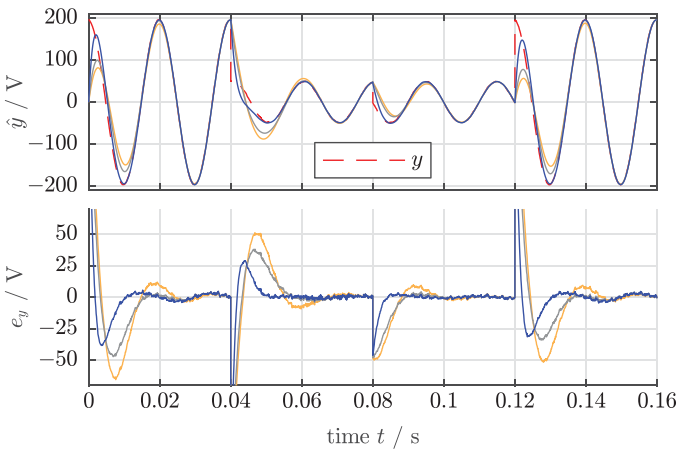

Fig. 7. Measurement results for Scenario (S_1). Comparison of the estimation performances of *single* mSOGI (——), sSOGI (——), and ANF (——) *without* FLL. Signals shown from top to bottom are: Fundamental input signal $y = y_1$ (- - -) and its estimate $\widehat{y} = \widehat{y_1}$ and estimation error $e_y = y_1 - \widehat{y_1}$.

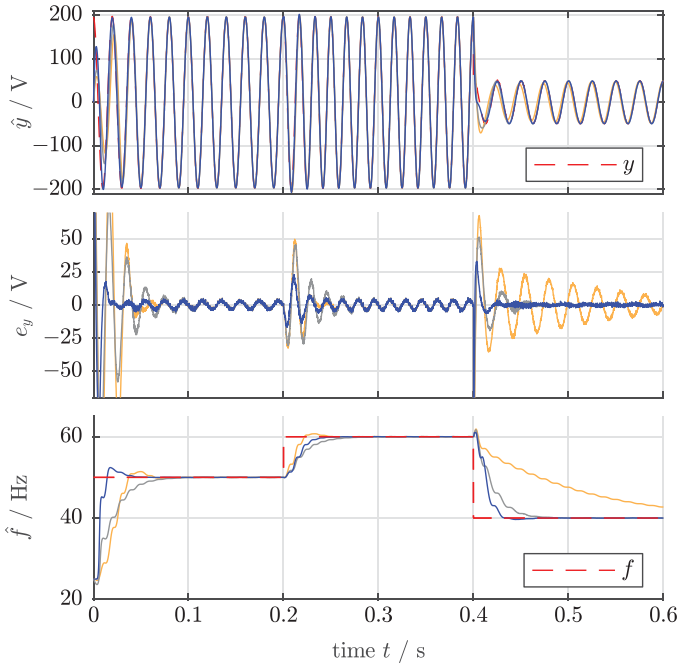

Fig. 8. Measurement results for Scenario (S_2). Comparison of the estimation performances of *single* mSOGI (——), sSOGI (——), and ANF (——) *with* FLL. Signals shown from top to bottom are: Fundamental input signal $y = y_1$ (- - -) and its estimate $\widehat{y} = \widehat{y_1}$; estimation error $e_y = y_1 - \widehat{y_1}$; frequency $f = \frac{\omega}{2\pi}$ (- - -) and its estimate $\widehat{f} = \frac{\widehat{\omega}}{2\pi}$.

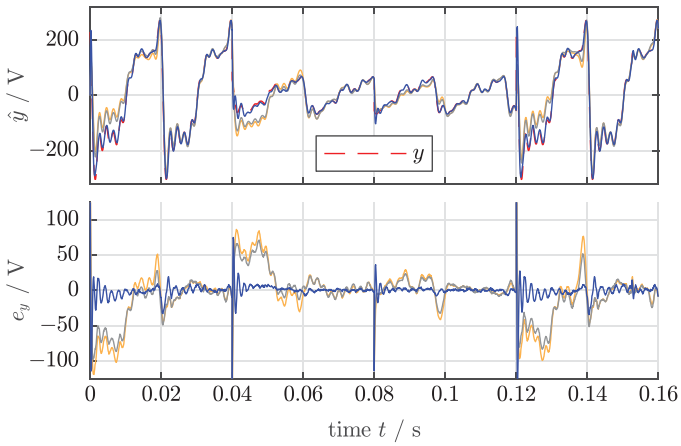

Fig. 9. Measurement results for Scenario (S_3): Comparison of the estimation performances of *parallelized* mSOGIs (——), sSOGIs (——), and ANFs (——) *without* FLL. Signals shown from top to bottom: Input signal y (- - -) and its estimate $\widehat{y}$ and estimation error $e_y = y - \widehat{y}$.

(with $a_1 = 194$). Whereas, for Scenarios (S_3) and (S_4), the input signals y have a significant harmonic distortion (10 harmonics). The parameters of the individual harmonics (amplitudes a_ν and frequencies f) of the signal y for Scenario (S_3) and for Scenario (S_4) are collected in Table II. Within the considered time intervals of each scenario, several jump-like changes in amplitude, phase and/or frequency occur. Hence, the input signal and its harmonic content changes abruptly and require *all* observers to "restart" their estimation process for each step-like change.

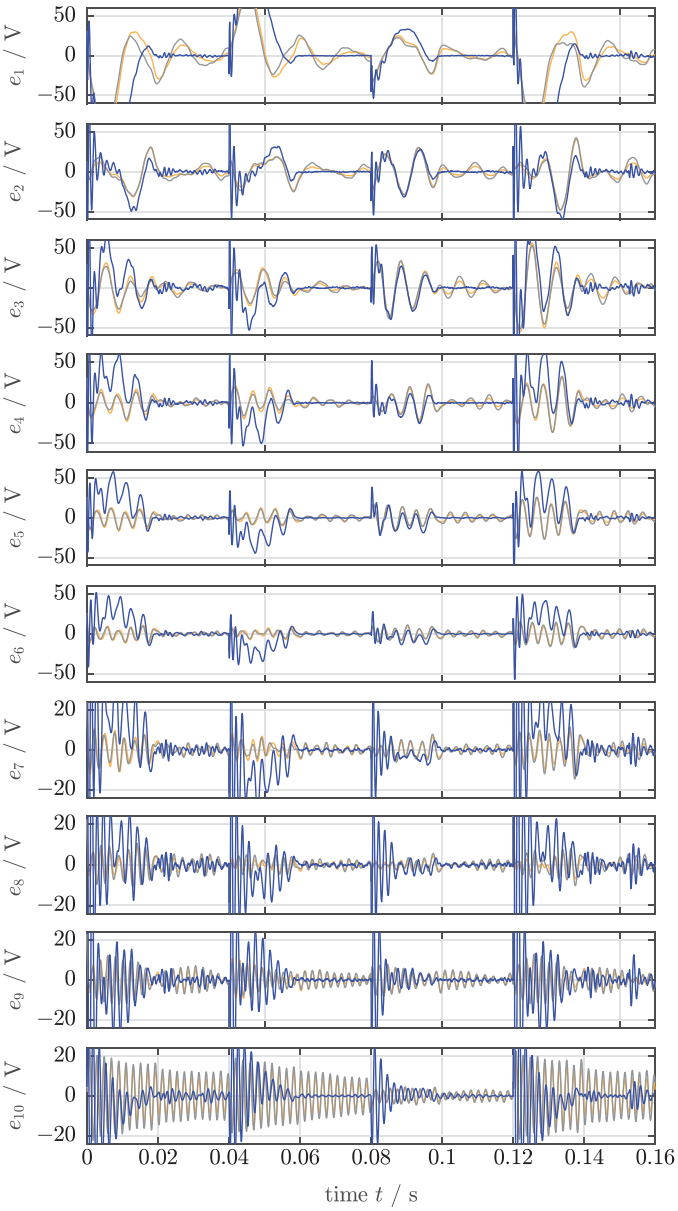

Fig. 10. Measurement results for Scenario (S_3): Comparison of the estimation performances of *parallelized* mSOGIs (——), sSOGIs (——), and ANFs (——) *with* FLL. Signals shown from top to bottom are: Harmonic estimation errors $e_1 = y_1 - \widehat{y}_1$ to $e_{10} = y_{10} - \widehat{y}_{10}$.

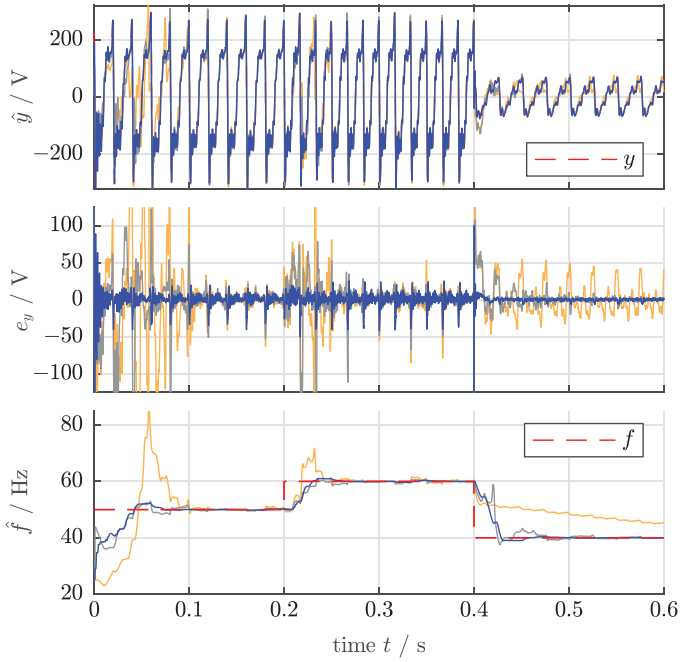

Fig. 11. Measurement results for Scenario (S_4): Comparison of the estimation performances of *parallelized* mSOGIs (——), sSOGIs (——), and ANFs (——) *without* FLL. Signals shown from top to bottom are: Harmonic signals y_1 to y_{10} (- - -) and their estimates $\widehat{y}_1$ to $\widehat{y}_{10}$ and harmonic estimation errors $e_1 = y_1 - \widehat{y}_1$ to $e_{10} = y_{10} - \widehat{y}_{10}$.

For a fair comparison, all three estimation methods are tuned in such a way that the best feasible estimation performance were achieved within their respective capability and tuning limits. All four results will be discussed in more detail in the next subsections.

A. Discussion of the Measurement Results for Scenario (S_1)

For scenario (S_1), only a *single* mSOGI, a single sSOGI, and a single ANF are implemented for *fundamental* signal estimation, respectively. The FLLs were implemented but the adaption was turned off, respectively. Fundamental and estimated angular frequency are identical for this scenario. Therefore, the estimation performances purely can be compared according to the respective observer tunings only. The fundamental signal $y = y_1$ undergoes step-like changes in amplitude, phase and amplitude and phase as described above.

The estimation performances of fundamental mSOGI (——), fundamental sSOGI (——), and fundamental ANF (——) are shown in Fig. 7. The first and second subplots show input signal $y = y_1$ (- - -) and its estimates $\widehat{y} = \widehat{y}_1$ and the estimation errors $e_y = y_1 - \widehat{y}_1$, respectively. All three observers are capable of estimating the input signal y. All estimation errors $e_y \to 0$ tend to zero after a certain time. The mSOGI (——) clearly outperforms the other two estimation methods in estimation accuracy and estimation speed for all three step-like changes of the input signal y at $t = 0.04,\ 0.08$, and 0.12 s. Estimation is completed in less than 20 ms. This is possibly due to the additionally introduced gain g_1 which gives the necessary degree of freedom in mSOGI design (recall discussion in Section II-B). The oscillations within first ($0 \leq t < 0.04$ s) and fourth ($0.12 \leq t \leq 0.16$ s) interval are identical for all estimation methods and are due to the grid emulator, which is not able to perfectly produce a constant amplitude for higher voltage levels.

B. Discussion of the Measurement Results for Scenario (S_2)

For Scenario (S_2), the respective FLLs for mSOGI, sSOGI, and ANF [as in Scenario (S_1)] are *activated* now. Signal *and* frequency estimation will be compared during this scenario. The considered fundamental signal y undergoes step-like frequency

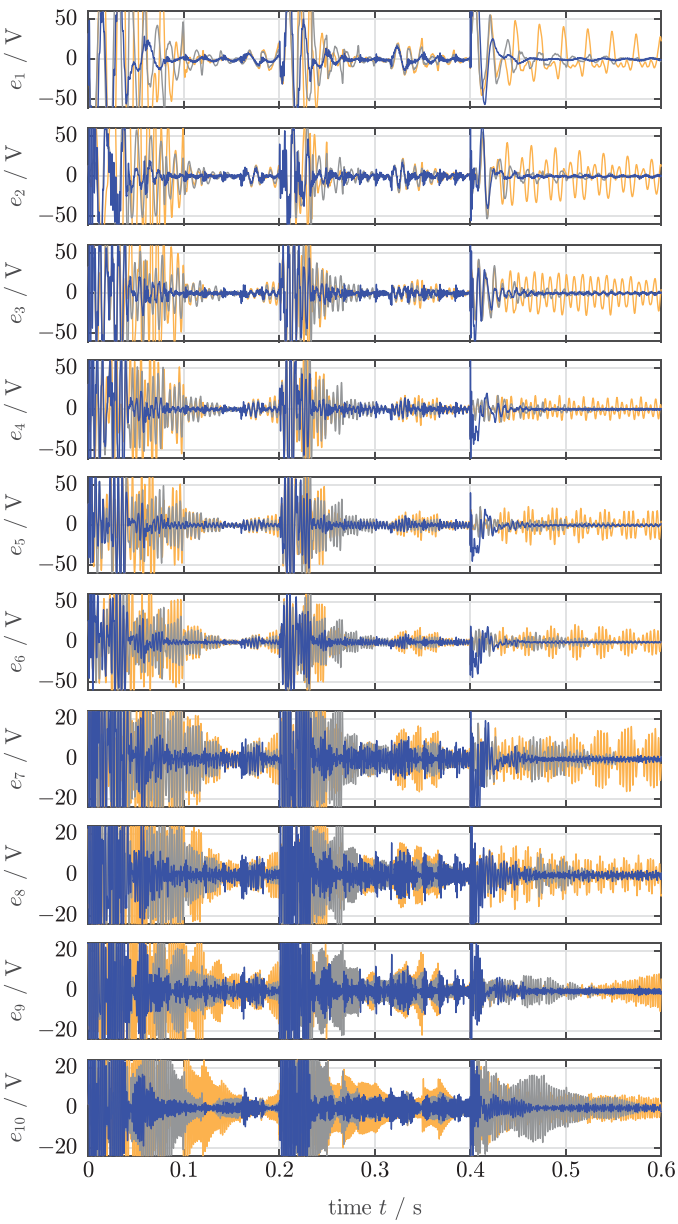

Fig. 12. Measurement results for Scenario (S_4): Comparison of the estimation performances of *parallelized* mSOGIs (——), sSOGIs (——), and ANFs (——) *without* FLL. Signals shown from top to bottom are: Harmonic estimation errors $e_1 = y_1 - \widehat{y}_1$ to $e_{10} = y_{10} - \widehat{y}_{10}$.

and amplitude changes as described above (see also Fig. 8). Fig. 8 illustrates the estimation performances of fundamental mSOGI with mFLL (——), fundamental sSOGI with sFLL (——), and fundamental ANF with FLL (——). The first, second, and third subplots show input signal $y = y_1$ (- - -) and its estimates $\widehat{y} = \widehat{y}_1$, the estimation errors $e_y = y_1 - \widehat{y}_1$ and fundamental frequency f (- - -) and its estimates $\widehat{f} = \frac{\widehat{\omega}}{2\pi}$, respectively. Again all three observers can estimate the input signal y. All estimation errors $e_y \to 0$ decay (almost) to zero after a certain time. Also for this experiment, the grid emulator induces undesired oscillations for large signal amplitudes, which

TABLE II
DATA OF INPUT SIGNAL y FOR SCENARIOS (S_3) AND (S_4)

Considered harmonics for both scenarios										
ν	1	2	3	4	5	6	7	8	9	10
Scenario (S_3): Constant frequency ($\omega(t) = 2\pi\,50\,\mathrm{Hz}$)										
• time interval $0 \le t < 0.04\,\mathrm{s}$:										
a_ν	194	34	67	46	36	29	29	22	23	19
• time interval $0.04 \le t < 0.08\,\mathrm{s}$ (amplitude jump):										
a_ν	49	21	16	0	9	7.5	7.5	5	0	6
• time interval $0.08 \le t < 0.12\,\mathrm{s}$ (phase jump):										
a_ν	49	21	16	0	9	7.5	7.5	5	0	6
• time interval $0.12 \le t \le 0.16\,\mathrm{s}$ (phase & ampl. jump):										
a_ν	194	34	67	46	36	29	29	22	23	19
Scenario (S_4): Varying frequency ($\omega(t) \neq$ const.)										
• time interval $0 \le t < 0.2\,\mathrm{s}$:										
a_ν	194	34	67	46	36	29	29	22	23	19
ω_ν			$\nu \cdot \omega$		with		$\omega = 2\pi\,50\,\mathrm{Hz}$			
• time interval $0.2 \le t < 0.4\,\mathrm{s}$ (frequency jump):										
a_ν	194	34	67	46	36	29	29	22	23	19
ω_ν			$\nu \cdot \omega$		with		$\omega = 2\pi\,60\,\mathrm{Hz}$			
• time interval $0.4 \le t \le 0.6\,\mathrm{s}$ (ampl. & freq. jump):										
a_ν	49	21	16	0	9	7.5	7.5	5	0	6
ω_ν			$\nu \cdot \omega$		with		$\omega = 2\pi\,40\,\mathrm{Hz}$			

deteriorates the estimation performance of all three estimation methods; in particular during the interval $0 \le t < 0.4$ s. Nevertheless, the mSOGI with mFLL (——) performs best with respect to estimation accuracy and estimation speed for both step-like changes of the input signal y (- - -) and frequency jumps f (- - -) at $t = 0.2$ and 0.4 s. For the mSOGI with mFLL, signal estimation and frequency adaption are completed within 30–40 ms. Especially, the estimation performance of the ANF with FLL (——) is very slow and does not reach the frequency asymptotically within the interval $0.4 \le t \le 0.6$ s. This is due to the missing gain normalization in the FLL adaption law for the ANF [3].

C. Discussion of the Measurement Results for Scenario (S_3)

Scenario (S_3) is more challenging. Now, the input signal y contains ten harmonics and undergoes amplitude, phase, and amplitude/phase jumps at $t_1 = 0.04$ s, $t_2 = 0.08$ s, and $t_3 = 0.12$ s, respectively [see description of (S_3) above]. Estimated frequency and real frequency coincide, i.e., $\widehat{\omega}(t) = \omega(t)$ for all $t \in [0{,}0.16\ \mathrm{s}]$. The FLLs are implemented but frequency adaption is *deactivated*, such that solely the signal estimation performances of the three estimation methods without FLL can be evaluated and compared. To be able to estimate the ten

harmonics, the observers consist of *ten parallelized* mSOGIs, sSOGIs, and ANFs, respectively. The measurement results are shown in Figs. 9 and 10.

In Fig. 9, estimated signals $\widehat{y}$ and estimation errors $e_y := y - \widehat{y}$ are shown for the *parallelized* mSOGIs (——), sSOGIs (——), and ANFs (——), respectively. All three estimation methods are somehow able to estimate the signal y correctly. But again, estimation accuracy and estimation speed of the parallelized mSOGIs are much better than those of parallelized sSOGIs and ANFs as can be seen in e_y. The estimation error tends to zero within 20 ms (or less) after all three step-like changes at $t_1 = 0.04$ s, $t_2 = 0.08$ s, and $t_3 = 0.12$ s, respectively. In contrast to that, the overall estimation accuracy and estimation speed of the parallelized sSOGIs (——) and parallelized ANFs (——) are rather bad and slow. After each step change, rapid and large changes in e_y occur over (almost) all 40 ms until the next jump in the input signal y happens.

Similar observations can be made by comparing the individual harmonic estimation performances in Fig. 10, where the harmonic estimation errors $e_\nu = y_\nu - \widehat{y}_\nu$ of the three estimation methods are shown for all harmonics $\nu \in \{1, \ldots, 10\}$. Also here, estimation speed and estimation accuracy of the parallelized mSOGIs (——) is better for (almost) all harmonic components and completed within 20ms. For higher-order harmonics (see e_7 to e_9 in Fig. 12), the difference in estimation speed is not as significant as it is for lower order harmonics. Note that, in general, the estimation accuracies of parallelized sSOGIs (——) and ANFs (——) exhibit significant oscillations and do not (always) tend to zero within 40ms. In particular, for the tenth harmonic component (see e_{10} in Fig. 10), parallelized sSOGIs (——) and ANFs (——) do not perform acceptable.

D. Discussion of the Measurement Results for Scenario (S_4)

Scenario (S_4) is the most challenging. The input signal y has again severe harmonic distortion (*ten* harmonics are considered) and is affected by frequency and amplitude/frequency jumps at $t_1 = 0.2$ s and $t_2 = 0.4$ s, respectively (recall description of (S_4) above). The FLLs for all three estimation methods are implemented and *activated*. The observers again comprise *ten parallelized* mSOGIs, sSOGIs, and ANFs, respectively. The results of Scenario (S_4) are shown in Figs. 11 and 12.

Fig. 11 shows estimated signals $\widehat{y}$, estimation errors $e_y := y - \widehat{y}$ and fundamental frequencies f (- - -) & its estimates $\widehat{f} = \frac{\widehat{\omega}}{2\pi}$ for the *parallelized* mSOGIs (——), sSOGIs (——), and ANFs (——), respectively. All three estimation methods are able to roughly estimate the input signal y. Again, the parallelized mSOGIs with mFLL outperform the other two estimation methods (see e_y in Fig. 11). The step-like frequency changes are estimated asymptotically by all three methods, but the transient responses of the individual FLLs differ much; e.g. the FLL of the parallelized ANFs (——) overshoots significantly and is not able to asymptotically estimate the frequency within the interval $[0.4s, 0.6s]$. Here, again, the beneficial effect of gain normalization in mFLL and sFLL become obvious. Noise sensitivity and oscillations are visible for all three estimation methods.

In Fig. 12, the harmonic estimation errors $e_\nu = y_\nu - \widehat{y}_\nu$ of all three methods are plotted for all ten harmonic components $\nu \in \{1, \ldots, 10\}$. Again, also for Scenario (S_4), estimation speed and estimation accuracy of the parallelized mSOGIs with mFLL (——) are better for (almost) all harmonic components (see e_1 to e_{10} in Fig. 12). The estimation accuracies of the parallelized sSOGIs (——) and ANFs (——) exhibit significant oscillations and do not tend to zero (in particular for higher harmonics). Their estimation performances are clearly not acceptable anymore. However, the difference in estimation speed is not as significant as it was for Scenario (S_3), which shows that frequency estimation in *general* remains the weakest part of grid state estimation (independently of the use of mSOGIs, sSOGIs, or ANFs) and has to be improved further (future work).

V. Conclusion

A mSOGI for the ν-th harmonic component and a mFLL for the parallelized mSOGIs have been proposed. The number ν can represent any positive not necessarily natural harmonic of an arbitrarily deteriorated input signal for which fundamental and higher harmonic components shall be estimated in real time. In contrast to the ν-th sSOGI in literature, the ν-th mSOGI allows (theoretically) for an arbitrarily fast estimation of the in-phase and quadrature signal of any specified harmonic component with prescribed settling time. This is possible due to an additionally introduced feedback gain in the mSOGI design. The proposed mFLL is equipped with a sign-correct AWU strategy and rate limitation. These modifications enhance the frequency estimation in such a way that the frequency estimate remains positive and bounded and does not change too quickly (independently of mFLL tuning or operating point). Moreover, both enhancements overcome the stability problem of the estimator when an sFLL is used. All measurement results presented for the four Scenarios (S_1)–(S_4) illustrate and verify the improved estimation performance of the parallelized mSOGIs with and without mFLL in comparison to parallelized sSOGIs and ANFs with and without sFLL, respectively.

Future work will focus on 1) further improvements of the mFLL (acceleration of frequency estimation and global stability analysis), 2) the extension of the presented results to three-phase signals (including dc offsets), and 3) the real-time estimation of positive, negative, and zero sequences of each harmonic component.

References

[1] F. Milano, F. Dörfler, G. Hug, D. J. Hill, and G. Verbič, "Foundations and challenges of low-inertia systems (invited paper)," in *Proc. Power Syst. Comput. Conf.*, 2018, pp. 1–25.

[2] P. Rodriguez, A. Luna, M. Ciobotaru, R. Teodorescu, and F. Blaabjerg, "Advanced grid synchronization system for power converters under unbalanced and distorted operating conditions," in *Proc. 32nd Annu. Conf. IEEE Ind. Electron.*, 2006, pp. 5173–5178.

[3] M. Mojiri, M. Karimi-Ghartemani, and A. Bakhshai, "Time-domain signal analysis using adaptive notch filter," *IEEE Trans. Signal Process.*, vol. 55, no. 1, pp. 85–93, Jan. 2007.

[4] R. S. R. Chilipi, N. A. Sayari, K. H. A. Hosani, and A. R. Beig, "Adaptive notch filter-based multipurpose control scheme for grid-interfaced three-phase four-wire DG inverter," *IEEE Trans. Ind. Appl.*, vol. 53, no. 4, pp. 4015–4027, Jul. 2017.

[5] G. Fedele, A. Ferrise, and D. Frascino, "Structural properties of the SOGI system for parameters estimation of a biased sinusoid," in *Proc. 9th Int. Conf. Environ. Elect. Eng.*, 2010, pp. 438–441.
[6] P. Rodriguez, A. Luna, I. Candela, R. Mujal, R. Teodorescu, and F. Blaabjerg, "Multiresonant frequency-locked loop for grid synchronization of power converters under distorted grid conditions," *IEEE Trans. Ind. Electron.*, vol. 58, no. 1, pp. 127–138, Jan. 2011.
[7] F. Muzi and M. Barbati, "A real-time harmonic monitoring aimed at improving smart grid power quality," in *Proc. IEEE Int. Conf. Smart Meas. Future Grids*, 2011, pp. 95–100.
[8] Z. Luo, M. Kaye, C. Diduch, and L. Chang, "Frequency measurement using a frequency locked loop," in *Proc. IEEE Energy Convers. Congr. Expo.*, pp. 917–921, Sep. 2011.
[9] J. Park, D. Lee, and T. L. Van, "Advanced single-phase SOGI-FLL using self-tuning gain based on fuzzy logic," in *Proc. IEEE ECCE Asia Downunder*, 2013, pp. 1282–1288.
[10] A. Kulkarni and V. John, "A novel design method for SOGI-PLL for minimum settling time and low unit vector distortion," in *Proc. 39th Annu. Conf. IEEE Ind. Electron. Soc.*, 2013, pp. 274–279.
[11] S. K. Panda and T. K. Dash, "An improved method of frequency detection for grid synchronization of DG systems during grid abnormalities," in *Proc. Int. Conf. Circuits, Power Comput. Technol.*, 2014, pp. 153–157.
[12] P. Cossutta, S. Raffo, A. Cao, F. Ditaranto, M. P. Aguirre, and M. I. Valla, "High speed single phase SOGI-PLL with high resolution implementation on an FPGA," in *Proc. IEEE 24th Int. Symp. Ind. Electron.*, 2015, pp. 1004–1009.
[13] Z. Xin, R. Zhao, P. Mattavelli, P. C. Loh, and F. Blaabjerg, "Reinvestigation of generalized integrator based filters from a first-order-system perspective," *IEEE Access*, vol. 4, pp. 7131–7144, 2016.
[14] K. R. Patil and H. H. Patel, "Modified dual second-order generalised integrator FLL for synchronization of a distributed generator to a weak grid," in *Proc. IEEE 16th Int. Conf. Environ. Elect. Eng.*, 2016, pp. 1–5.
[15] S. Golestan, J. M. Guerrero, and J. C. Vasquez, "A robust and fast synchronization technique for adverse grid conditions," *IEEE Trans. Ind. Electron.*, vol. 64, no. 4, pp. 3188–3194, Apr. 2017.
[16] J. Matas, H. Martin, J. de la Hoz, A. Abusorrah, Y. A. Al-Turki, and M. Al-Hindawi, "A family of gradient descent grid frequency estimators for the SOGI filter," *IEEE Trans. Power Electron.*, vol. 33, no. 1, pp. 5796–5810, Jul. 2018.
[17] I. Ralev, A. Klein-Hessling, B. Pariti, and R. W. D. Doncker, "Adopting a SOGI filter for flux-linkage based rotor position sensing of switched reluctance machines," in *Proc. IEEE Int. Elect. Mach. Drives Conf.*, 2017, pp. 1–7.
[18] F. Xiao, L. Dong, L. Li, and X. Liao, "A frequency-fixed SOGI-based PLL for single-phase grid-connected converters," *IEEE Trans. Power Electron.*, vol. 32, no. 3, pp. 1713–1719, Mar. 2017.
[19] H. Yi, X. Wang, F. Blaabjerg, and F. Zhuo, "Impedance analysis of SOGI-FLL-based grid synchronization," *IEEE Trans. Power Electron.*, vol. 32, no. 10, pp. 7409–7413, Oct. 2017.
[20] S. Golestan, S. Y. Mousazadeh, J. M. Guerrero, and J. C. Vasquez, "A critical examination of frequency-fixed second-order generalized integrator-based phase-locked loops," *IEEE Trans. Power Electron.*, vol. 32, no. 9, pp. 6666–6672, Sep. 2017.
[21] S. Golestan, J. M. Guerrero, and J. C. Vasquez, "Three-phase PLLs: A review of recent advances," *IEEE Trans. Power Electron.*, vol. 32, no. 3, pp. 1894–1907, Mar. 2017.
[22] Z. Dai, Z. Zhang, Y. Yang, F. Blaabjerg, Y. Huangfu, and J. Zhang, "A fixed-length transfer delay-based adaptive frequency locked loop for single-phase systems," *IEEE Trans. Power Electron.*, vol. 34, no. 5, pp. 4000–4004, May 2019.
[23] A. E. Karkevandi and M. J. Daryani, "Frequency estimation with anti-windup to improve sogi filter transient response to voltage sags," in *Proc. 6th Int. Istanbul Smart Grids Cities Congr. Fair*, 2018, pp. 188–192.
[24] X. He, H. Geng, and G. Yang, "Reinvestigation of single-phase FLLs," *IEEE Access*, vol. 7, pp. 13178–13188, 2019.
[25] L. Råde and B. Westergren, *Springers Mathematische Formeln: Taschenbuch für Ingenieure, Naturwissenschaftler, Informatiker, Wirtschaftswissenschaftler*. Berlin, Germany: Springer, 2000.
[26] R. Teodorescu, M. Liserre, and P. Rodríguez, *Grid Converters for Photovoltaic and Wind Power Systems*. Chichester, U.K.: Wiley, 2011.
[27] S. Reza, M. Ciobotaru, and V. G. Agelidis, "Accurate estimation of single-phase grid voltage fundamental amplitude and frequency by using a frequency adaptive linear Kalman filter," *IEEE J. Emerg. Sel. Topics Power Electron.*, vol. 4, no. 4, pp. 1226–1235, Dec. 2016.
[28] M. S. Reza, M. Ciobotaru, and V. G. Agelidis, "Accurate estimation of single-phase grid voltage parameters under distorted conditions," *IEEE Trans. Power Del.*, vol. 29, no. 3, pp. 1138–1146, Jun. 2014.
[29] Z. Dai, W. Lin, and H. Lin, "Estimation of single-phase grid voltage parameters with zero steady-state error," *IEEE Trans. Power Electron.*, vol. 31, no. 5, pp. 3867–3879, May 2016.
[30] H. Ahmed, S. Amamra, and M. H. Bierhoff, "Frequency-locked loop based estimation of single-phase grid voltage parameters," *IEEE Trans. Ind. Electron.*, vol. 66, no. 11, pp. 8856-8859, Nov. 2019.
[31] W. M. Wonham, *Linear Multivariable Control: A Geometric Approach*, 3rd ed. Berlin, Germany: Springer-Verlag, 1985.
[32] C. M. Hackl, *Non-Identifier Based Adaptive Control in Mechatronics: Theory and Application*. Berlin, Germany: Springer-Verlag, 2017.
[33] X. He, H. Geng, and G. Yang, "A generalized design framework of notch filter based frequency-locked loop for three-phase grid voltage," *IEEE Trans. Ind. Electron.*, vol. 65, no. 9, pp. 7072–7084, Sep. 2018.

Christoph M. Hackl (M'12–SM'16) was born in 1977 in Mannheim, Germany. He received the B.Sc., Dipl.-Ing., and Dr.-Ing. (Ph.D.) degrees in electrical engineering from Technical University of Munich (TUM), Munich, Germany, in 2003, 2004, and 2012, respectively.

Since 2004, he has been teaching electrical drives, power electronics, and mechatronic and renewable energy systems. Since 2014, he has been the Head of the research group Control of Renewable Energy Systems (CRES) at TUM. In 2018, he became a Professor of Electrical Machines and Drives and the Head of the Laboratory for Mechatronic and Renewable Energy Systems (LMRES) at the Munich University of Applied Sciences (MUAS), Munich, Germany. His research interests include nonlinear, adaptive, and optimal control of electric, mechatronic, and renewable energy systems.

Markus Landerer was born in 1988 in Ebersberg, Germany. He received the B.Sc. and M.Sc. degrees in electrical engineering, with focus on controls and energy transmission/energy systems, from the Technical University of Munich (TUM), Munich, Germany, in 2013 and 2016, respectively. He is currently working toward the Ph.D. degree in electrical engineering at TUM.

From 2016 to 2018, he was a Research Associate within the research group Control of Renewable Energy Systems (CRES) at TUM. Since 2019, he is a Research Associate within Laboratory for Mechatronic and Renewable Energy Systems (LMRES) at the Munich University of Applied Sciences (MUAS), Munich. His research interests include nonlinear and adaptive control and modeling of electrical and renewable energy systems.